Molecular Crystals and Liquid Crystals

Publication details, including instructions for authors and subscription information:
http://www.tandfonline.com/loi/gmcl20

From the Synclinic to the Anticlinic Smectic Phases: a Deuterium NMR and Diffusion NMR Study

Mario Cifelli [a], Valentina Domenici [a] & Carlo Alberto Veracini [a]

[a] Dipartimento di Chimica e Chimica Industriale, Università degli Studi di Pisa, Pisa, Italy

Version of record first published: 31 Aug 2006

To cite this article: Mario Cifelli, Valentina Domenici & Carlo Alberto Veracini (2005): From the Synclinic to the Anticlinic Smectic Phases: a Deuterium NMR and Diffusion NMR Study, Molecular Crystals and Liquid Crystals, 429:1, 167-179

To link to this article: http://dx.doi.org/10.1080/15421400590930908

Mol. Cryst. Liq. Cryst., Vol. 429, pp. 167–179, 2005

ISSN: 1542-1406 print/1563-5287 online
DOI: 10.1080/15421400590930908

Taylor & Francis
Taylor & Francis Group

From the Synclinic to the Anticlinic Smectic Phases: a Deuterium NMR and Diffusion NMR Study

Mario Cifelli
Valentina Domenici
Carlo Alberto Veracini
Dipartimento di Chimica e Chimica Industriale, Università degli Studi di Pisa, Pisa, Italy

The behaviour of the ^2H NMR line-width throughout the whole mesophasic range of the ferroelectric liquid crystal "1-methylheptyl 4′-(4″-n-decyloxybenzoyloxy) biphenyl-4-carboxylate" (10B1M7) is here reported and discussed.

Static Fringe Field NMR Diffusometry measurements from the isotropic to the anticlinic phase have been performed leading to a significant result concerning the tumbling diffusional coefficient ($D_\perp$).

These results have been compared to X-Ray measurements and ^2H NMR line-widths in order to explain the peculiar behaviour occurring at the transition between the ferroelectric (FLC) and the antiferroelectric (AFLC) liquid crystalline phases.

Keywords: diffusion; dynamics; ^{2}H NMR; liquid crystals; line-width

INTRODUCTION

There has been recently much effort devoted to elucidating the structure and polar properties of FLC and AFLC phases. Continuous experimental work and many different theoretical models have been put forward to explain the microscopic nature of the organization of chiral phases and the molecular reasons of the transition from the synclinic to the anticlinic phases.

We thank the Italian MIUR for partial financial support. We also thank Prof. B. Zalar and Prof. R. Blinc for helpful discussions and Prof. R. Richardson for the X-Ray contribution.

Address correspondence to Carlo Alberto Veracini, Dipartimento di Chimica e Chimica Industriale, Università degli Studi di Pisa, via Risorgimento 35, 56126 Pisa, Italia. E-mail: verax@dcci.unipi.it

In a previous investigation on the smectogen object of the present work [1], 10B1M7, partially deuterated on the aromatic core (both on the phenyl and biphenyl moieties) a progressive Deuterium NMR (DNMR) line-width increase was observed entering the SmC^* phase from the SmA one. This line-width increase is not linked to this particular mesogen: looking to the literature this phenomenon has been already observed in different cases [2], as a tilted phase is formed from a SmA one, in DNMR spectra as well as in ^{13}C ones.

However, no particular attention has been dedicated to the occuring of this line broadening in the chiral phase and only in some cases the Goldstone mode has been invoked as a dynamic effect that could explain this line-width increase [3].

In reference [1] we were able not only to point out this line-width increase in the synclinic phase but also a further decrease entering the anticlinic antiferroeletric smectic phase.

In principle either static disorder or dynamic modulations could be responsible of the observed line broadening in tilted phases, but what has still to be rationalized is the further decrease of the line-width as the anticlinic phase is formed. This line-width behaviour, happening so generally in NMR of chiral smectic phases and still not completely clarified, could be linked to some fundamental aspects of the structural change occurring at the FLC – AFLC phase transition.

In this paper, with the impression that this behaviour could be of interest in elucidating the structure of chiral subphases, we have undertaken different experiments on the 10B1M7 smectogen. Starting from a detailed investigation of the DNMR line-width behaviour of the fully deuterated achiral chain of the smectogen, we then exploited the angular dependence of the deuterium quadrupolar coupling of the alfa methyl of the achiral chain to obtain further informations. Moreover, SAXS measurements of the smectic layer spacing, as well as an evaluation of the out of plane component of the molecular translational diffusion, by means of ^1H stray field diffusometry [4], have been carried out throughout the smectic phases of the smectogen under investigation, in order to bring forward some deeper knowledge about the phase transitions.

Finally we will try to rationalize and explain these experimental results in a complessive discussion.

EXPERIMENTAL

Deuterium NMR Line-widths

The ^2H NMR experiments on the sample 10B1M7-d_{21}were carried out on a 7.05 T Varian VXR-300 spectrometer, working at 46.04 MHz for deuterium. The 90° pulse was 22 μs.

The sample was microscopically aligned within the magnets by slow cooling from the isotropic phase and the spectra were recorded every two degrees allowing 10 minutes for thermal equilibration. The temperature was stable within 0.2 degrees.

The ^{2}H NMR measurements on the sample 10B1M7-d_2, deuterated on the phenyl fragment as indicated in Ref. [5], were carried out on a 15 T Varian600 spectrometer, working at 92.06 MHz for deuterium. The spectra were acquired by using the quadrupolar echo sequence (90_x-τ-90_y-τ-ACQ), with a τ delay of 25 μs and a 90° pulse of 8 μs. The sample was microscopically aligned within the magnets by slow cooling from the isotropic phase and the spectra were recorded every five degrees from 130° to 30°, allowing 10 minutes for thermal equilibration. The temperature was stable within 0.2 degrees.

SAXS Measurements

The diffraction measurements were made using copper Kα X-rays (1.54 Å), from a 1.5 kW sealed tube with other wavelengths removed using a nickel filter and a graphite monochromator. The diffraction pattern was detected using a multi-wire area detector [6]. It was placed at 840 mm from the sample with an evacuated path so that a Q (scattering vector) range from 0.03 Å^{-1} to 0.5 Å^{-1} was covered. The sample to detector distance was calibrated using a silver behenate standard [7] and the Q values calculated from the scattering angle, 2θ, ($Q = 4\pi \sin\theta$). Since the samples were not aligned, the scattering was regrouped so that pixels at the same Q were averaged and the maximum of each diffraction peak was determined numerically and used to calculate its mean scattering vector, Q_B. The relative precision of the Q_B values was generally better than 0.01% although the absolute accuracy would be about 1%. The software for viewing and analysing the X-ray scattering was developed with PV-WAVE [8].

Diffusion Measurements

All the diffusion measurements have been performed in the Static Fringe Field (SFF) gradient of a 9.4 T Magnex (UK) super-conducting magnet. The exact position corresponded to a proton resonance frequency of 235 MHz (located 112 mm below the iso-centre) where the nominal field gradient strength in the vertical ($z//B_0$) direction of the magnet is 58 T/m. This position and gradient were identified from a magnetic field plot supplied by Magnex and verified using stray field imaging of thin planar samples.

The radio-frequency probe was home made with a 90° pulse of 1.1 to 1.5 μs, dependant on the sample loading and temperature. Hence, the excited slice in the sample varied from about 1 to 0.7 mm; a distance far greater than the average molecular displacement during the measurement. The temperature was measured using a PT100 resistance thermometer and controlled by a Chemagnetics temperature controller. The temperature stability was better than $+/-0.5$°C.

The 10B1M7 sample has been homogenously aligned with the smectic A phase director parallel to the SFF direction cooling it from the isotropic phase.

RESULTS

Deuterium NMR Line-width of 10B1M7 d_{21}

The sample under study is the 10B1M7-d_{21}, with C10 achiral chain fully deuterated. The synthesis was performed following the route reported in Ref. [1] and a complete analysis of the dynamic behaviour in the SmA phase of this compound has been just published in [9]. Deuterium NMR spectra have been collected slowly cooling down the sample from the isotropic phase to the semicrystalline SmJ*. The spectra are shown in Figure 1. The transition temperatures of this deuterated compound are slightly lower than those of the non deuterated sample, which are: 124.5°C for isotropic-SmA, 105.4°C for SmA-SmC*, 75.9°C for SmC*-SmC*ferri, 69°C for SmC*ferri-SmC*anti, and 47.8°C for the SmC*anti-SmJ* phase transition. Despite many deuterated sites in the SmA phase almost all the quadrupolar couplings can be assigned to the deuteria in the achiral chain, assuming a monotone decrease of the quadrupolar splitting along the chain.

In the SmA phase deuterium signals for C1 and C2 moieties overlap in a broad signal, while C5 and C6 probably turn out to be overlapped in a quite sharp signal. Line-width for all the quadrupolar doublets turned out to be constant as the temperature decreases.

At the SmA-SmC* phase transition all the line-widths starts to broaden and the splittings of the inner methylenes (reasonably from C1 to C6) rapidly coalesce in a wide and complex structure, nevertheless the outer methylenes (from C7 to C9) and the methyl (C10) give still rise to enough resolved quadrupolar doublets. This broadening is typical for SmC* phases and has been already observed in some other ferroelectric smectogens [2,10].

The peculiarity of this sample is the sudden decrease of the doublets linewidths as the SmC*ferri phase is reached and lines remain narrow till the high ordered SmJ* phase is entered. This behaviour is clearly depicted in Figure 2 for the C7–C10 sites of the achiral chain.

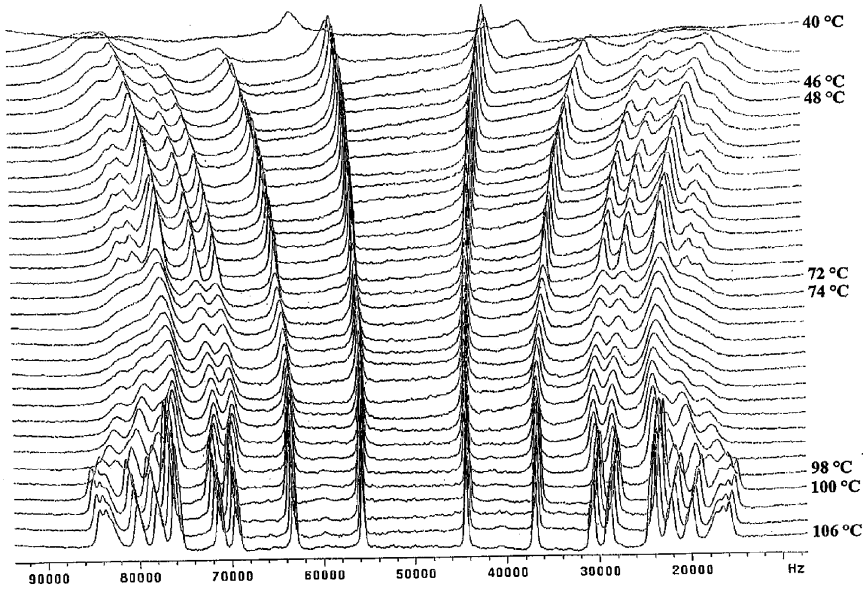

FIGURE 1 ^{2}H NMR spectra of 10B1M7-d_{21} in function of temperature (°C) from the SmA (on the bottom) to the crystal (on the top).

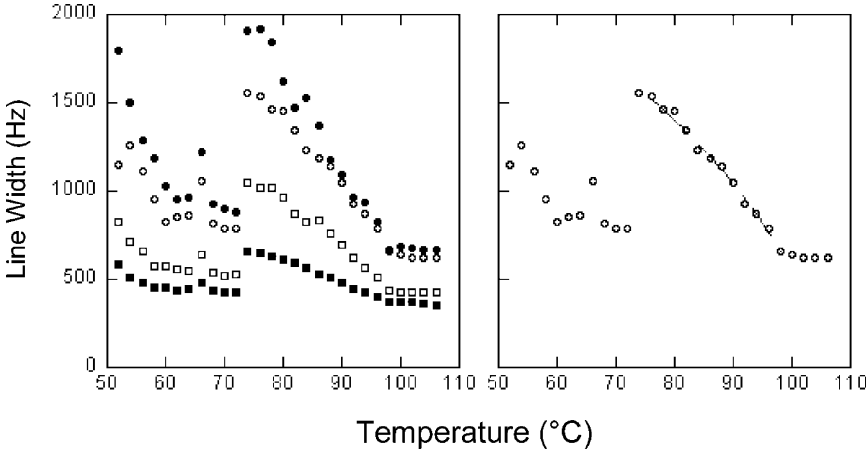

FIGURE 2 Left. DNMR line-widths of the last four sites of the C10 achiral chain of 10B1M7. The symbols represent respectively: (●) C7, (○) C8, (■) C9 and (□) C10. Right. C8 DNMR line width; the SmC* phase behaviour has been fitted with the Landau-DeGennes equation with $\beta = 0.56$.

Previous studies on the same compound, performed by means of ^{13}C NMR by Nishiyama *et al.* [11] reveal the same behaviour which is particularly evident for aromatic signals: the line broadening in the SmC* phase, and also SmC*anti one, contrasts with the relative sharp peaks obtained in the SmC*ferri. The linewidth discontinuities among these smectic phases probably are correlated with different dynamic behaviours, as it is suggested by ^{13}C T_1 trends obtained for this compound [11] and for an other ferroelectric one [2]. The purpose of this paper is to give a more detailed explanation of these complex phenomena.

Static Fringe Field NMR Diffusometry

Static Fringe field diffusometry proposed by Kimmich and coworkers [12] is a valuable method for measuring self-diffusion in systems with small diffusion coefficients and/or short nuclear spin relaxation times [4]. It exploits the large, steady and very stable magnetic field gradient surrounding a conventional high field magnet in place of the switched field gradients generated using current windings used in PFG. The method, has been used by Kimmich *et al.* to measure diffusion in polymer melts [12]; by Feweier *et al.* in super-cooled fluids [13] and Karakatsanis and Bayerl in phospholipids bilayers [14]. It has been used by Vilfan and co-workers to measure self-diffusion of the nematic phase of 4-n-pentyl-4′-cyanobiphenyl (5CB) both in the bulk and confined in controlled porous glasses [15].

Methodology

Recently SFF diffusometry has been succesfully exploited to determine the translational self-diffusion along the phase director in the nematic and smectic A phase of the 4-n-octyloxy-4′-cyanobiphenyl (8OCB) [16]. The method there reported takes advantage of a double stimulated echo approach in order to remove contributions to the echo decays due to spin relaxation and dipolar correlation effects [17]. Two stimulated echo experiments are considered:

$$\left(\frac{\pi}{2}\right)_x - \tau - \left(\frac{\pi}{2}\right)_x - (\Delta - \tau) - \left(\frac{\pi}{2}\right)_x - \tau - echo \tag{1}$$

and

$$\left(\frac{\pi}{2}\right)_x - \left(\frac{\tau+\delta}{2}\right) - \pi_y - \left(\frac{\tau-\delta}{2}\right) - \left(\frac{\pi}{2}\right)_y - (\Delta - \tau) - \left(\frac{\pi}{2}\right)_y - \left(\frac{\tau-\delta}{2}\right) - \pi_y - \left(\frac{\tau+\delta}{2}\right) - \left(\frac{\pi}{2}\right)_y - echo \tag{2}$$

Here $\left(\frac{\pi}{2}\right)_{x/y}$ and π_y are a 90° and 180° excitation pulses of relative phase x or y and τ, δ and $(\Delta - \tau)$ are periods of magnetisation evolution in the transverse plane and storage in the longitudinal direction respectively.

As the two experiments are performed as a function of the diffusion time Δ, in the case $\Delta \gg \tau > \delta$ (that is a typical experimental condition), the diffusion coefficient measured along the gradient direction can be determined from the ratio of the two echo amplitudes decays:

$$\frac{A^{STE}}{A_{5p}^{STE}} = \exp[-(\gamma G)^2 D_{||}^G \Delta(\tau^2 - \delta^2)] \tag{3}$$

where A^{STE} and A_{5p}^{STE} are the echo amplitude of the pulse sequence (1) and (2) respectively, γ is the magnetogyric ratio, $D_{||}^G$ is the diffusion coefficient parallel to the field gradient direction and G is the strength of the static gradient.

In the present case a variant of the method has been considered, that takes into account possible cross relaxations effects that can affect the stimulated echo decay. As demonstrated by Furó and Dvinskikh [18], in the case of a two spin system with a chemical shift difference of $\Delta\omega$, longitudinal cross relaxation affects the stimulated echo amplitude in a way that it decays bi-exponentially as the diffusion time Δ increases.

$$\begin{aligned} A^{STE}(\tau, \delta) = &(B_1 + C_1 \cos(\Delta\omega \cdot \tau)) \exp(\lambda_+ \Delta) \\ &+ (B_2 + C_2 \cos(\Delta\omega \cdot \tau)) \exp(\lambda_- \Delta) \end{aligned} \tag{4}$$

$$\begin{aligned} A_{5p}^{STE}(\tau, \delta) = &(B_1 + C_1 \cos(\Delta\omega \cdot \delta)) \exp(\lambda_+^{5p} \Delta) \\ &+ (B_2 + C_2 \cos(\Delta\omega \cdot \delta)) \exp(\lambda_-^{5p} \Delta) \end{aligned} \tag{5}$$

with $\lambda_\pm = \rho_+ - 2\gamma G D_{||}^G \tau \pm \mu - c^{DCE}$, $\lambda_\pm^{5p} = \rho_+ - 2\gamma G D_{||}^G \delta \pm \mu - c^{DCE}$. The coefficient c^{DCE} has been added to take into account the dipolar correlation contribution to the echo decays [16] while ρ_+, μ, B_i and C_i are parameters dependent on the terms of the longitudinal cross relaxation matrix for a two spin system as reported in references [18,19]. Dipolar correlation and longitudinal cross relaxation related terms will not be discussed further. What is worth to notice for the present aim is that the self-diffusion coefficient $D_{||}^G$ can be extracted from Eqs. (4) and (5) considering that:

$$\lambda_\pm - \lambda_\pm^{5p} = -2\gamma G D_{||}^G (\tau - \delta) \tag{6}$$

Consequently the diffusion coefficient $D_{||}^{G}$ can be determined:

$$D_{||}^{G} = -(\lambda_{\pm} - \lambda_{\pm}^{5p})/[2\gamma G(\tau - \delta)] \quad (7)$$

In fact, all the terms that depend on dipolar correlation and longitudinal relaxation are removed by the difference, while the transverse relaxation contribution is held constant, as τ is kept constant [16].

Experimental Results

Stimulated echo decays of experiments (1) and (2) have been collected as a function of the diffusion time Δ at different temperatures. The echoes have been acquired with 40 scans and a repetition time of five seconds. Fixed values of $\tau = 50\,\mu s$ and $\delta = 10\,\mu s$ were used, whereas Δ was varied in the range 5–100 ms to 5–800 ms as the temperature decreased.

While in the isotropic phase the echo amplitudes decays in a single exponential fashion, as the liquid crystal phase form the decay becomes bi-exponential. In Figure 3 echo amplitude decays collected

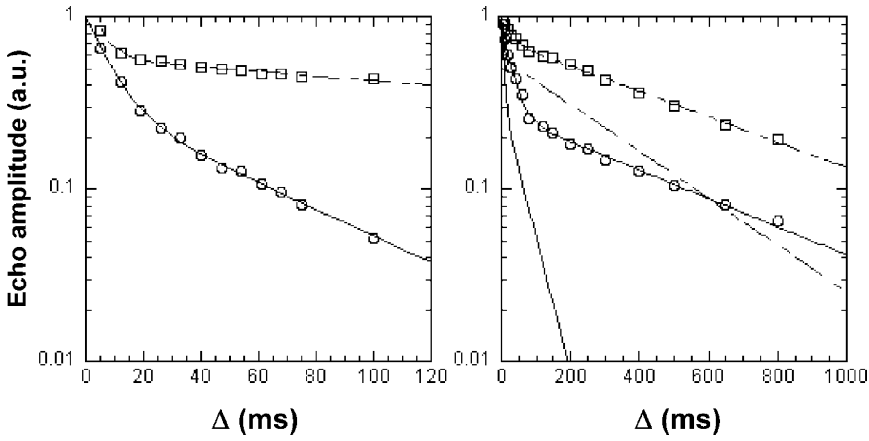

FIGURE 3 On the left: Double Exponential Echo decays at T = 375 K. The empty circles and the empty squares represent the STE echo decay and the STE + 180° pulses decay respectively. The lines show the best fitting obtained with a bi-exponential fitting. On the right: Double Exponential Echo decays at T = 337 K. The empty circle and the empty squares represent the STE echo decay and the STE + 180° pulses decay respectively. The lines show the best fitting obtained with a bi-exponential. The echo decays at T = 375 K are shown for comparison; the different effect of the diffusion attenuation effect is evident.

at T = 375 K and T = 337 K are reported as an example. It can be easily noticed the relevant difference in the decays between the smectic sinclinic phase (Fig. 3, on the left) and the anticlinic smectic phase (Fig. 3, on the right).

As the echo amplitudes decay in a single exponential way in the isotropic phase, the diffusion coefficient could be determined following the method reported in reference [16]. On the other hand, in order to determine the out of plane diffusion coefficient in the smectic phases we followed the method described in the previous section.

The echo amplitude decays have been well fitted using a simplified version of Eqs. (8) and (9):

$$A^{STE}(\tau,\delta) = P_1 \exp(\lambda_+ \Delta) + P_2 \exp(\lambda_- \Delta) \tag{8}$$

$$A^{STE}_{5p}(\tau,\delta) = P_3 \exp(\lambda^{5p}_+ \Delta) + P_4 \exp(\lambda^{5p}_- \Delta) \tag{9}$$

From the best fitting parameters $\lambda_\pm$'s the diffusion coefficient $D^G_{||}$ has been determined using Eq. (7). The values obtained are reported in Table 1.

In Figure 4 are graphically reported the whole set of data collected as a function of temperature, with the corresponding error bars. A discontinuous step at T = 389 K denotes the effect of the uniaxial smectic A formation; $D^G_{||}$ turns from D_{iso}, the isotropic diffusion coefficient, to $D_{||}$ that expresses the diffusion process parallel to the phase director in the principal axis system of the smectic A phase. Hence, despite the layer formation, phase, near the phase transition the *rod-like* 10B1M7 molecules diffuse more easily along the phase director that in the non ordered isotropic.

However, the more interesting result of this data set can be individuated in the sharp decrease of the measured diffusion coefficient going from the synclinic to the anticlinic phase (compare the diffusion

TABLE 1 Out of Plane Component of the Diffusion Tensor Determined from the Lambda Fitting Coefficients. The Values Reported are in Units of $10^{-11}\,m^2/s$

Temp (K)	$D_{||}$ Lambda (+)	$D_{||}$ Lambda (−)	$D_{||}$ Average
387	5.2	5.1	5.15
375	3.7	3.3	3.5
357	2.4	2.7	2.55
345	1.6	1.9	1.75
339	0.06	0.04	0.050
337	0.06	0.05	0.055

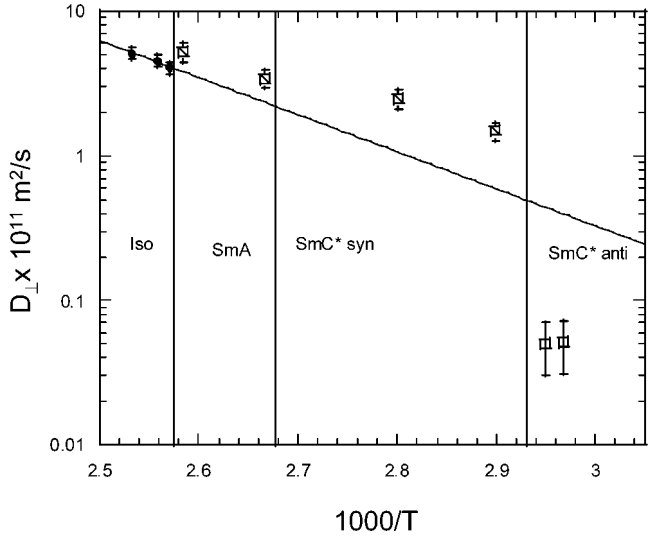

FIGURE 4 Diffusion coefficients in the isotropic phase and along the out of plane direction in the smectic phases of 10B1M7. The diffusion coefficients in the LC phases are the average value reported in Table 1. The error bars in the isotropic and synclinic phases has been estimated about 10%, of the corresponding value, whereas, in the anticlinic phase, the error rises to 40% due to the lower value of the diffusion coefficient. The full line represents an Arrhenius fitting of the isotropic diffusion with an activation energy of 58 kJ/mol.

coefficient at T = 345 K and T = 339 K). This sudden decrease of $D_{||}^{G}$ can be correlated to the layer organization that changes from a synclinic to an anticlinc arrangement. $D_{||}^{G}$ hence drops of more than one order of magnitude in the SmC* antiferroelectric (AFE) phase, with respect to the synclinic SmC* ferroelectric one. This behaviour should be explained by the fact that an anticlinic arrangement of the smectic layers relevantly hinders the out of plane diffusional process. An analogous result has been already determined from the investigation of interlayer molecular exchange by means of deuterium NMR in the SmC* AFE phase of the chiral smectogen MHPOBC [20]. In that case the probability per unit time of an interlayer jump through the layers, w has been evaluated and related to the macroscopic diffusion coefficient by the relation $D_{||}^{G} = w/d^2$, where d^2 is the layer thickness. The $D_{||}^{G}$ value reported is comparable to one the determined in the present work [20].

CONCLUSIONS

As shown in Figures 1 and 2, the line-width depends on the quadrupolar splitting and therefore on the CD bond nematic order. The increase in linewidth, which could be related to the increase of the tilt angle in the SmC* phase, can be fitted with a Landau De Gennes equation with a β value that spans from 0.8 to 0.56 going from the C7 to the C10 carbon sites of the achiral chain under study. Such a line broadening happens always, as in the present case, when the director makes an angle $\theta \neq 0$ with the static magnetic field direction. Whenever this angle is affected by some orientation the linewidth increases and the higher is the quadrupolar splitting the higher turns to be the linewidth increase.

In principle this distribution could be ascribed either to some static disorder or to some dynamic modulation. In fact, as shown by the SAXS measurements (see Fig. 5), the structure of the mesophase undergoes only changes as far as the layer spacing or the tilt angle are concerned.

However what is important to stress is not only the linewidth increase in the SmC* phase but the further decrease as soon as the anticlinic phase occurs. It is therefore extremely unlikely that by lowering the temperature we can pass from a disordered static situation to a more ordered one since the static disorder can only be frozen by lowering the temperature.

In fact, as shown by the quadrupolar echo experiments (reported in Fig. 6) the line broadening is dynamic in nature. This broadening, moreover, cannot arise from Goldstone modes [21]: *phasons* do not

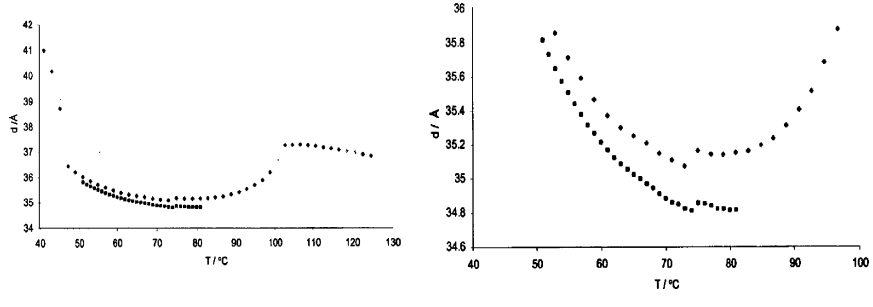

FIGURE 5 SAXS Measurements on 10B1M7 in the smectic phases. On the right the figure is zoomed in at the Ferro-Antiferroelectric transition. Upper points refer to measurements during cooling process, lower points refer to the warming process in a range of temperature from 50°C to about 80°C.

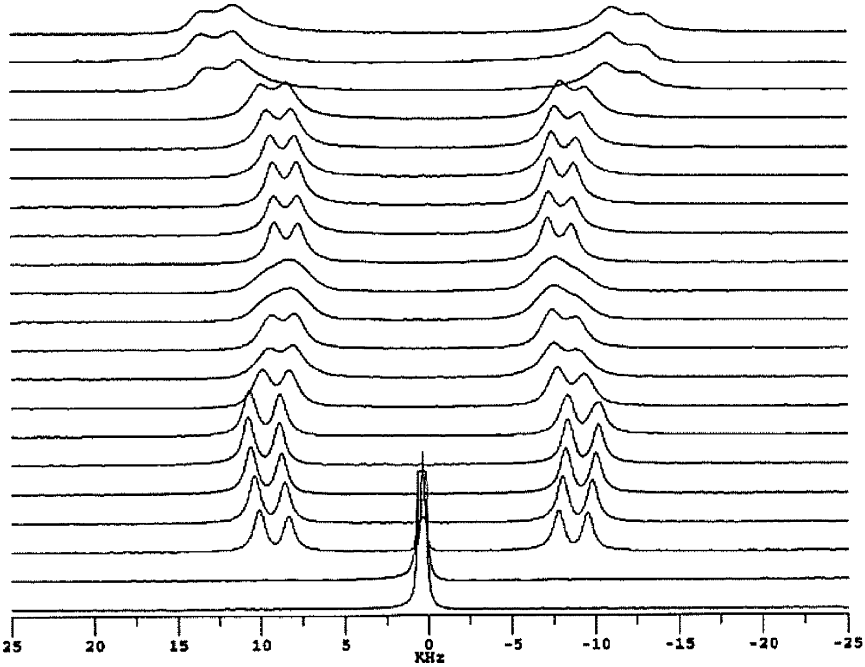

FIGURE 6 ^{2}H NMR spectra recorded with the quadrupolar echo sequence of 10B1M7-d_2 in function of temperature (°C) from the isotropic at 130°C (on the bottom) to the crystal at 30°C (on the top) phases, every 5 degrees interval.

imply modification of the tilt angle. Amplitude fluctuations of the tilt angle helix (*amplitudons*) could explain the observed line broadening.

In summary going from synclinic to anticlinic phases there is only a poor change in the layer spacing (tilt angle). On the other hand, the diffusion is strongly affected, changing by two orders of magnitude; soft-modes undergo a significant change too.

REFERENCES

[1] Catalano, D., Cavazza, M., Chiezzi, L., Geppi, M., & Veracini, C. A. (2000). *Liq. Cryst.*, *27*, 621–627.
[2] Yoshizawa, A., Yokoyama, A., Kikuzaki H., & Hirai, T. (1993). *Liq. Cryst.*, *14*, 513–523.
[3] Dong, R. Y. (1997). *Nuclear magnetic resonance of liquid crystals*, Springer: New York.
[4] Geil, B. (1998). *Concept Magnetic. Res.*, *10*(5), 299.
[5] Catalano, D., Cifelli, M., Geppi, M., & Veracini, C. A., (2001). *J. Phys. Chem. A*, *105*, 34.

[6] Bateman, J. E., Connolly, J. F., Stephenson, R., Flesher, A. C., Bryant, C. J., Lincoln, A. D., Tucker, P. A., & Swanton, S. W. (1987). *Nucl. Inst. and Meth. in Hys. Res.*, *A259*, 506.
[7] Huang, T. C., Toraya, H., Blanton, T. N., & Wu, Y. (1993). *J Appl. Cryst.*, *26*, 180.
[8] Supplied by Visual Numerics. http://www.vni.com/products/wave/index.html.
[9] Dong, R. Y., Chiezzi, L., & Veracini, C. A. (2002). *Phys. Rev. E*, *65*(4), 1716–1723.
[10] Catalano, D., Chiezzi, L., Domenici, V., Geppi, M., Veracini, C. A., Dong, R. Y., & Fodor Csorba, K. (2002). *Macromol. Chem. Phys.*, *203*, 1594.
[11] Nishiyama, I., Saito M., & Yoshizawa, A. (1995). *Mol. Cryst. Liq. Cryst.*, *263*, 123–129.
[12] Kimmich, R., Unrath, W., Schnur, G., & Rommel, E. (1991). *J. Magn. Reson.*, *103*, 136.
[13] Feweier, T., Isfort, O., Geil, B., Fujara, F., & Weingärtner, H. (1996). *J. Chem. Phys.*, *105*, 5757.
[14] Karakatsanis, P. & Bayerl, T. M. (1996). *Phys. Rev. E*, *54*(2), 1785.
[15] Vilfan, M., Apih, T., Gregorovič, A., Zalar, B., Lahajnar, G., Žumer, S., Hinze, G., Böhmer, R., & Althoff, G. (2001). *Magn. Reson. Imaging*, *19*, 433.
[16] Cifelli, M., McDonald, P. J., & Veracini, C. A. *Phys. Chem. Chem. Phys.*, to be published.
[17] Kimmich, R., Fischer, E., Callaghan, P., & Fatkullin, N. (1995). *J. Magn. Reson. A*, *117*, 53.
[18] Dvinskikh, S. V. & Furò, I. (2000). *J. Magn. Reson.*, *146*, 283.
[19] Ernst, R. R., Bodenhausen, G., & Wokaun, A. (1987). "*Principles of nuclear magnetic resonance in one and two dimensions*", Clarendon Press: Oxford.
[20] Zalar, B., Gregorovič, A., & Blinc, R. (2000). *Phys. Rev. E*, *62*(1), R37.
[21] Musevic, I., Blinc, R., & Zeks, B. (2000). *The physic of ferroelectric and antiferroelectric liquid crystals*, World Scientific: Singapore.